

---

# BA-Net: Dense Bundle Adjustment Network

---

Chengzhou Tang, Ping Tan

School of Computing Science, Simon Fraser University  
 {cta73,pingtang}@sfu.ca

## Abstract

This paper introduces a neural network to solve the structure-from-motion (SfM) problem via feature bundle adjustment (BA), which explicitly enforces multi-view geometry constraints in the form of feature reprojection error. The whole pipeline is differentiable, so that the network can learn suitable feature representations that make the BA problem more trackable. Furthermore, this work introduces a novel depth parameterization to recover dense per-pixel depth. The network first generates some bases depth maps according to the input image, and optimizes the final depth as a linear combination of these bases via feature BA. The bases depth map generator is also learned via end-to-end training. The whole system nicely combines domain knowledge (i.e. hard-coded multi-view geometry constraints) and machine learning (i.e. feature learning and basis depth map generator learning) to address the challenging SfM problem. Experiments on large scale real data prove the success of the proposed method.

## 1 Introduction

In the past few years, deep learning has become the state-of-the-art in high-level [30, 44, 24, 26] and low-level [13, 52] vision tasks. It also starts to surpass most conventional methods in some middle-level tasks such as optical flow [14, 27], stereo matching [28, 39], and monocular depth estimation [16, 32, 53]. Some recent works attempt to resolve Structure-from-Motion (SfM) [43] using deep learning techniques, but most of them do not enforce the geometric constraints between the 3D structures and camera motion in their network. For example, in the paper [50], the scene depth and camera motion are estimated by two individual sub-network branches. In comparison, almost all conventional SfM algorithms [1, 51, 43, 17, 11] jointly optimize scene structures and camera motion via the Bundle-Adjustment (BA) algorithm [48, 3], which minimizes the geometric [1, 51, 43] or photometric [18, 17, 11] error through the Levenberg-Marquett (LM) algorithm.

This paper formulates BA as a differentiable layer, the BA-Layer, to bridge the gap between classic SfM and recent deep learning approaches. To this end, we leverage a feed-forward neural network to learn the damping factor in the LM algorithm which makes all involved computation differentiable. Furthermore, unlike conventional BA with geometric or photometric error, our BA-layer minimizes the distance between reprojected CNN features. Our novel ‘feature BA’ takes CNN features of two images as input and computes camera motion and scene structures. Feature BA is desirable, because it has been observed [18, 17] that the geometric BA does not exploit all image information, while the photometric BA is sensitive to moving objects, exposure or white balance changes, etc. Most importantly, our BA-layer can back-propagate loss from camera pose and scene structures to learn appropriate features that are most suitable for structure-from-motion and bundle adjustment. In this way, our network hard-codes the multi-view geometry constraints in the BA layer, and learns suitable features for SfM from training data.

We strive to estimate a dense per-pixel depth, because dense depth maps capture complete surface shapes and are critical for many tasks such as semantic segmentation, object detection, and robot navigation. A major challenge in solving dense per-pixel depth in a network is to find a compact pa-

parameterization of the depth map. Direct per-pixel depth parameterization is computational expensive, which makes the network training intractable. So we train a network to generate a set of basis depth maps for any input image, and represent the result depth map as a linear combination of these bases. The combination coefficients will be optimized in the BA-Layer together with camera motion. This novel parameterization guarantees a smooth depth map with good consistency with object boundaries. It also reduces the number of unknowns and makes dense BA possible in neural networks. Similar depth parameterization is introduced in a concurrent work, CodeSLAM [6]. The major difference is that our method learns the basis depth map generator through the gradients back-propagated from the BA-Layer, while CodeSLAM learns the generator separately and uses its results for a standalone pose optimization component. Thus, our basis depth map generator has the chance to be better trained for the SfM problem. Furthermore, we use different network structures for depth parameterization. CodeSLAM employs a variational auto-encoder(VAE), while we use a standard encoder-decoder structure, which enables us to use the same backbone network for both features and depths, making joint learning of features and basis depth map generator possible.

To demonstrate the effectiveness of our method, we construct a dataset contains nearly 55K training and 2K testing pairs from ScanNet [10]. Our method outperforms the DeMon [50] as well as conventional methods with geometric [37, 2] and photometric BA [18]. We also conduct the experiments on KITTI dataset [20] and demonstrate that our method also outperforms the recently proposed unsupervised methods [8, 56]. Finally, we evaluate the importance of each building block in ablation studies and show that feature learning and differentiable BA-Layer are critical to the whole network.

## 2 Related Work

**Monocular Depth Estimation Networks** Estimating depth from a monocular image is an ill-posed problem because an infinite number of possible scenes may have produced the same image. Before the raise of deep learning based methods, some works predict depth from a single image based on MRF [40, 41], semantic segmentation [31], or manually designed features [25]. Eigen et al. [16] proposed a multi-scale approach for depth prediction with two CNNs, where a coarse-scale network first predicts the scene depth at global level and then a fine-scale network will refine local regions. This approach was extended in [15] to handle semantic segmentation and surface normal estimation as well. Recently, Laina et al. [32] proposed to use ResNet [24] based structure to predict depth, and Xu et al. [54] constructed multi-scale CRFs for depth prediction. In comparison, we exploit monocular image depth estimation network for depth parameterization, which only produces a compact depth representation and the final result is optimized with multi-view constraints for improved quality.

**Structure-from-Motion Networks** Recently, some works exploit CNNs to resolve the structure-from-motion problem. Handa et al. [23] solved the camera motion by a network from a pair of images with known depth. Zhou et al. [56] employed two CNNs for depth and camera motion estimation respectively, where both CNNs are trained jointly by minimizing the photometric loss in an unsupervised manner. Wang et al. [8] implemented the direct method [45] as a differentiable component to compute camera motion after scene depth is estimated by the method in [56]. Ummenhofer et al. [50] predicted the camera motion and scene depth from flow features, which help to make it generalizing better to unseen data. However, motion and depth are solved by two separate network branches, multi-view geometry constraints between motion and depth are not enforced.

Our method belongs to this category. Unlike all previous works, we propose the BA-Layer to simultaneously compute the camera motion and scene depth from CNN features, which explicitly enforces multi-view geometry constraints. Furthermore, we proposed to minimize a ‘feature errors’ instead of the photometric error in [56, 8] to enhance robustness.

## 3 Bundle Adjustment Revisit

Before introducing our BA-Net architecture, we revisit the classic BA to have a better understanding about where the difficulty is and why feature BA and feature learning is desirable. We only introduce the most relevant content and refer the audience to [49, 3] for a comprehensive introduction. Given images  $\mathcal{I} = \{\mathcal{I}_i | i = 1 \cdots N_i\}$  and a set of feature points  $\mathcal{Q} = \{\mathbf{q}_k | k = 1 \cdots N_k\}$ , the geometric BA algorithm [49, 3] jointly optimizes camera pose parameters  $\mathcal{T} = \{\mathbf{T}_i | i = 1 \cdots N_i\}$  and point

parameters  $\mathcal{P} = \{\mathbf{P}_j | j = 1 \cdots N_k\}$  by minimizing the reprojection error:

$$\mathbf{x} = \operatorname{argmin} \sum_{k=1}^{N_k} \|e_g(\mathbf{x})\|, \quad (1)$$

where the geometric error

$$e_g(\mathbf{x}) = \pi(\mathbf{T}_i, \mathbf{P}_j) - \mathbf{q}_k,$$

measures the distance between a projected scene point and its corresponding feature point. The function  $\pi$  projects scene points to image space, and  $\mathbf{x} = \{\mathcal{T}, \mathcal{P}\}$  is the vector that contains all camera and point parameters. The general strategy to minimize Equation (1) is the Levenberg-Marquardt (LM) [38, 35] algorithm. At each iteration, the LM algorithm computes a update  $\Delta \mathbf{x}$  to the solution by minimizing:

$$\Delta \mathbf{x} = \operatorname{argmin} \|J(\mathbf{x})\Delta \mathbf{x} + E(\mathbf{x})\|_2^2 + \lambda \|D(\mathbf{x})\Delta \mathbf{x}\|_2^2. \quad (2)$$

Here,  $E(\mathbf{x}) = [e_1(\mathbf{x}), e_2(\mathbf{x}) \cdots e_{N_k}(\mathbf{x})]$ , and  $J(\mathbf{x})$  is the Jacobian of  $E(\mathbf{x})$ ,  $D(\mathbf{x})$  is a non-negative diagonal matrix, typically the square root of the diagonal of the approximated Hessian matrix  $J(\mathbf{x})^\top J(\mathbf{x})$ . The parameter  $\lambda$  is a non-negative parameter that controls the strength of regularization. The special structure of the parameters in BA motivates the use of Schur Complement trick [7] where a reduced camera system is first solved and points are then updated via back-substitution.

This geometric BA with reprojection error is the golden standard in structure-from-motion in the last two decades, but with two main drawbacks:

- Only image information conforming to the respective feature types, typically image corners, blobs, or line segments, is utilized.
- Features have to be matched to each other, which often result in a lot of outliers, and a robust outlier rejection like RANSAC is required.

Recently, the direct methods [18, 17, 11] propose the ‘photometric BA’ algorithm to eliminate feature matching and directly minimize the photometric error (pixel intensity difference) of reprojected pixels, which replace the geometric error as:

$$e_p = I_i(\pi(\mathbf{T}_i, \mathbf{D}_j)) - I_1(\mathbf{p}_j), \quad (3)$$

where  $\mathbf{D}_j$  is the inverse depth value of pixel  $\mathbf{p}_j$  anchored at the keyframe  $I_1$ . The image frame  $I_i$  is a nearby frame to the keyframe. These direct methods have the advantages of using all pixels with sufficient gradient magnitude. They have demonstrated superior performance, especially at less textured scenes. However, these methods also have some drawbacks:

- They are sensitive to initialization as demonstrated in [36, 46] because the photometric error greatly increases the degree of non-convexity [17].
- They are sensitive to camera exposure and white balance changes. An automatic photometric calibration is required [17, 19].
- They are more sensitive to outliers such as moving objects.

## 4 The BA-Net Architecture

To deal with the above challenges, we propose a ‘feature BA’ algorithm which minimizes the feature error of reprojected pixels:

$$e_f(\mathbf{x}) = F_i(\pi(\mathbf{C}_i, \mathbf{D}_j)) - F_1(\mathbf{p}_j), \quad (4)$$

where  $\mathcal{F} = \{F_i | i = 1 \cdots N_i\}$  are feature pyramids of images  $\mathcal{I} = \{I_i | i = 1 \cdots N_i\}$ . Like the photometric BA, our feature BA considers more pixels than corners or blobs. Furthermore, it has the potential to learn more suitable features for SfM to deal with exposure changes, moving objects, etc.

We aim to learn features suitable for SfM through back-propagation, instead of using pre-trained CNNs features for image classification as in [9]. Therefore, it is crucial to design a differentiable optimization layer, our BA layer, to solve the minimization problem, so that the loss information can be back-propagated. The BA layer infers both camera poses  $\mathcal{C}$  and dense depth map  $\mathcal{D}$  during forward pass and back-propagates the loss from  $\mathcal{C}$  and  $\mathcal{D}$  to the feature pyramids  $\mathcal{F}$  to learn suitable features.

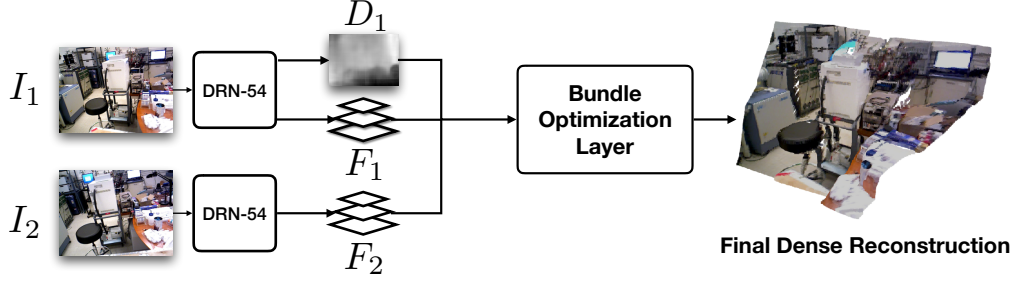


Figure 1: Overview of our BA-Net structure, which consists of a DRN-54 [55] as the backbone network, a **Depth Parameterization** sub-network that generates compact depth parameterization, a **Feature Pyramids** that extract multi-scale feature maps, and a **Bundle Adjustment Layer** that optimizes both the depth map and the camera poses through a novel differentiable LM algorithm.

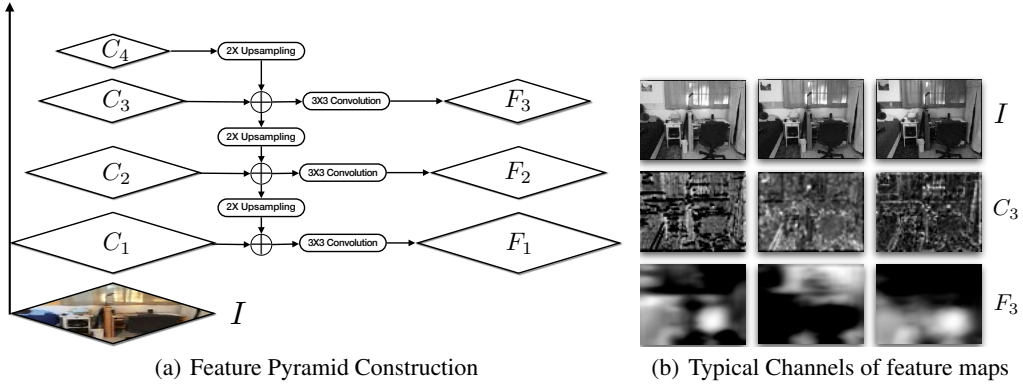


Figure 2: A feature pyramid and some typical channels from different feature maps.

#### 4.1 Overview

As illustrated in Figure 1, our BA-Net takes two images as inputs and then feed them to the backbone DRN-54. We use DRN as the backbone because it replaces max-pooling with convolutional layers and generate smoother feature maps, which is desirable for BA. Note the conventional DRN is memory inefficiently due to the high resolution feature maps after dilation convolutions. We replace the dilation convolution with ordinary convolution with strides to address this issue. After DRN is the depth parameterization sub-network that generates multiple basis depth maps for the frame  $I_1$ . The final depth is represented as a linear combination of these bases. A feature pyramid is then build for each input image, which are the inputs for the BA-Layer. Finally, the BA-Layer optimizes camera poses and depths jointly by minimizing the feature error defined in Equation (4). Thanks for our differentiable LM algorithm, the whole pipeline is end-to-end trainable.

#### 4.2 Feature Pyramid

The feature pyramid learns a suitable feature for the BA-Layer. Similar to the feature pyramid networks (FPN) for object detection [33], we exploit the inherent multi-scale, pyramidal hierarchy of deep convolutional networks to construct feature pyramids. A top-down architecture with lateral connections is applied to propagate richer context information from coarser scales to finer scales. Thus, our feature BA will have a larger convergence radius.

As shown in Figure 2(a), we construct the feature pyramid from the backbone DRN-54 network. Denote the last residual blocks of conv1, conv2, conv3, conv4 in DRN-54 as  $\{C_1, C_2, C_3, C_4\}$ , with strides  $\{1, 2, 4, 8\}$  respectively. We upsample a feature map by a factor of 2, and bilinear interpolation is applied for smoother feature maps. We then concatenate the upsampled map with the feature map in the next level. This procedure is iterated until the finest level. Finally, we apply a  $3 \times 3$  convolution

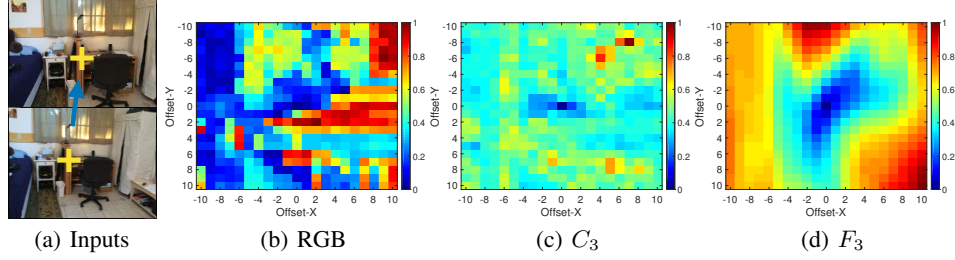


Figure 3: Feature distance maps defined over raw pixel values, pretrained CNN feature  $C_3$ , or our learned feature  $F_3$ . Our learned feature produces smoother cost function to facilitate optimization.

on the concatenated feature maps to reduce the dimensionality to 128 for a good balance between expressiveness and computational complexity, which generates the final feature map  $\{F_1, F_2, F_3\}$ .

We visualize some typical channels, e.g. the pretrained DRN  $C_3$  and our learned  $F_3$  in Figure 2(b). It is evidential that, after training with BA-Layer, the feature pyramid becomes smoother and each channel correpondences to different type of regions in the image. Note that our feature pyramids have higher resolution than FPN to facilitate precise alignment.

To have a better understanding about how BA optimization benefits from our learned feature, we illustrate different feature distance in Figure 3. The distance between the yellow cross in the top image in Figure 3 (a) and all pixels in the neighbour of its corresponding point in the bottom image Figure 3 (a) is visualized in (b), (c), and (d). All distances are normalized to  $[0, 1]$  and visualized as a heatmap. The RGB distance  $e_p$  in (b) has no clear global minimum, which makes the photometric BA sensitive to initialization [18, 17]. The feature distance measured by  $C_3$  of pretrained DRN-54 has both global and local minimum. Finally, the feature distance measured by our learned feature  $F_3$  has clear global minimum and smooth basin, which is helpful in gradient based optimization such as LM algorithm.

### 4.3 Bundle Adjustment Optimization Layer

After building feature pyramids  $\mathcal{F}$  for all images, we optimize camera poses and dense depth map by minimizing the feature distance in Equation (4). Following the conventional SfM principle, we optimize Equation (4) using the Levenberg-Marquardt (LM) algorithm. However, the original LM algorithm is non-differentiable for two difficulties:

- The iterative computation terminates when specified convergence threshold is reached. This if-else based termination strategy makes the output  $\mathbf{x}$  non-differentiable with respect to the input  $\mathcal{F}$  [12].
- In each iteration, it updates the damping factor  $\lambda$  based on the current value of the objective function. It raises  $\lambda$  if a step fails to reduce the objective function; otherwise it reduces the  $\lambda$ . This if-else makes  $\mathbf{x}$  non-differentiable with respect to  $\mathcal{F}$ .

When the solution  $\mathbf{x}$  is non-differentiable with respect to  $\mathcal{F}$ , feature learning by back-propagation becomes impossible. The first difficulty has been stuided in [12] and the authors propose to fix the number of iterations, which is referred as ‘incomplete optimization’. Besides making the optimization differentiable, this ‘incomplete optimization’ technique also reduces memory consumption because the number of iterations is usually fixed at a small value.

The second difficulty has never been studied. Pervious works mainly focus on gradient descent [12] or quatratic minimization [4, 42]. In this section, we propose a simple yet effective approach to soften the if-else decision and yelds a differentiable algorithm. We send the current objective function value to a feed-forward network to predict  $\lambda$ . This technique not only makes the optimization differentiable, but also learns to predict a better damping factor  $\lambda$ , which gaurantees that the optimziation will converged to a better solution with fewer iterations.

To start with, we illustrate a single iteration of the LM optimization as a diagram in Figure 4(a) and interpret intermediate variables as network nodes. During the *forward* pass, we predict the update solution  $\mathbf{x}$  from the feature  $\mathcal{F}$  and damping factor  $\lambda$ :

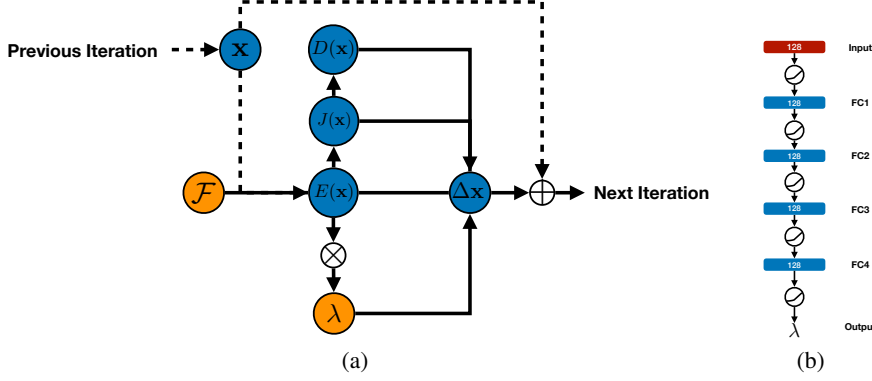


Figure 4: (a): A single iteration of the differentiable LM and (b): the fully-connected network to predict damping factor  $\lambda$ .

- We receive the solution  $\mathbf{x}$  from last iteration, and compute current feature differences  $E(\mathbf{x})$  as in Equation (4);
- Then we compute the Jacobian matrix of  $E(\mathbf{x})$  respect to  $\mathbf{x}$ , and  $D(\mathbf{x})$  is the diagonal matrix of  $J(\mathbf{x})^T J(\mathbf{x})$ ;
- To predict the damping factor  $\lambda$ , we use global average pooling to aggregate the absolute value of  $E(\mathbf{x})$  over all pixels for each feature channel, and get an  $n$  dimensional feature vector. Then a feed-forward network uses this feature vector as input and outputs  $\lambda$ ;
- Finally, the update  $\Delta \mathbf{x}$  to the current solution is computed as:

$$\Delta \mathbf{x} = (J(\mathbf{x})^T J(\mathbf{x}) + \lambda D(\mathbf{x}))^{-1} J(\mathbf{x})^T E(\mathbf{x}).$$

To simplify the description, we denote the solution  $\Delta \mathbf{x}$  as a function about features  $\mathcal{F}$ , damping factor  $\lambda$ , and the solution  $\mathbf{x}$  from last iteration:

$$\Delta \mathbf{x} = \mathcal{G}(\mathcal{F}, \lambda, \mathbf{x}). \quad (5)$$

All the intermediate variable nodes are connected with matrix operation or generated from neural networks. So the function Equation (5) is differentiable, which makes the back-propagation possible through the whole pipeline.

The feed-forward network that predicts  $\lambda$  is shown in Figure 4(b). We stack four fully-connected layers to predict it from a 128 dimensional input feature vectors. We use ReLU as activation function to make sure  $\lambda$  is a non-negative value. Following the photometric BA [18, 17], we optimize Equation (4) using a coarse-to-fine strategy over the feature pyramid. We apply the differentiable LM algorithm for 5 iterations at each feature pyramid level, therefore 15 iterations in total.

#### 4.4 Dense Depth Parameterization

Dense per-pixel depth is useful, but parameterizing a depth map by a per-pixel depth value is impractical. Firstly, it introduces too many parameters to be optimized. For example, an image of  $320 \times 240$  pixels results in 76.8k parameters. Secondly, in the beginning of training, when depth or motion prediction is still poor, many pixels will become invisible in the other view according to the predicted depth. So little information can be back-propagated to improve the network, which makes training difficult.

To deal with these problems, we use the network for monocular image depth estimation as a compact parameterization, rather than using it as an initialization like in [47]. We use a standard encoder-decoder architecture for monocular depth learning [32]. We modify the last convolutional feature maps to 120 dimensions and use them as depth bases for optimization. The depth map is generated by the last convolutional layer of the decoder, which is:

$$D = \text{ReLU}(\mathbf{w}^T B). \quad (6)$$

Here,  $D$  is the  $h \times w \times 1$  depth map,  $B$  is a  $h \times w \times 128$  tensor, representing 128 depth map bases generated from network,  $\mathbf{w}$  is the linear combination weights of these bases to be optimized.

in BALayer, and ReLU is the activation function that guarantee the depth is positive. Once the depth basis  $B$  is generated from network, we fix  $B$  and use  $\mathbf{w}$  as the depth parameterization for BA optimization. Therefore, the feature error becomes:

$$e_f = F_2(\pi(\mathbf{T}_i, \text{ReLU}(\mathbf{w}^\top B))) - F_1(\mathbf{p}_j). \quad (7)$$

To further speedup convergence, we learn an initial depth map  $D_0$  by a 1D convolution on the bases  $B$ , i.e.  $D_0 = \alpha(\mathbf{w}_0^\top B)$ . The initial weights  $\mathbf{w}_0$  can be learned as a convolutional filter.

## 4.5 Training

The BA-Net learns the feature pyramids, bases depths generator, and the damping factor predictor in a supervised manner. We apply the following commonly used loss for training, though more sophisticated ones might be designed.

**Camera Pose Loss** For each pair, the camera rotation loss is the distance between rotation quaternion vectors  $\mathcal{L}_{rotation} = \|\mathbf{q} - \mathbf{q}^*\|$ . Similarly, translation loss is the Euclidean distance between prediction and groundtruth in metric scale,  $\mathcal{L}_{translation} = \|\mathbf{t} - \mathbf{t}^*\|$ .

**Depth Map Loss** For each dense depth map we applies the berHu Loss [57]  $\mathcal{B}$  as in [32].

We train the networks by only initializing the back-bone netowrk from DRN [55], and the whole pipeline is trained with ADAM [29] with initial learning rate 0.001, and the learning rate is divided by two when we observe plateaus.

## 5 Experiments

### 5.1 Dataset

**ScanNet** ScanNet [10] is a large-scale indoor dataset with 1513 sequences in 706 different scenes. Camera poses and depth maps are not perfect, because they are obtained via RGBD reconstruction. The raw data is recorded from a structured light depth camera, which returns absolute depth values, thus the metric scale is known in the whole dataset.

To sample image pairs for training, we apply a simple filtering process. To avoid image pairs with large pose or depth error, we filter out pairs with a large photo-consistency error. We also filter out image pairs, if less than 50% of the pixels from one image is visible in the other image. We also discard a pair if their roundness score [5] is less than 0.001.

We split the datasets into training and testing sequences. The training set contains 1413 sequences and the test set contains the rest 100 sequences. For training we sample a total of 547991 image pairs from training sequences. For testing we generate a set of 2000 image pairs from the testing sequences.

**KITTI** KITTI [20] is a widely used benchmark dataset collected by car-mounted cameras and a LIDAR sensor on streets. It contains 61 scenes belonging to the "city", "residential", and "road" categories. Eigen et al. [16] selects 28 scenes for testing and 28 scenes from the remaining for training. In this paper, to make a fair comparison with previous methods, we use the same data split as Eigen for training and testing.

Since pose groundtruth is unavailable from the KITTI raw dataset, we generate camera poses from LibVISO2 [21] as groundtruth and discard poses with large error. To evaluate the camera poses, we follow [56, 8] to meausre the Absolute Trajectory Error on sequence 9 and sequence 10 from KITTI odometry data. In this experiment, we create short sequences of 5 frames by first generate 5 two-view reconstruction from our BA-Net and then align the two-view reconstruction in a unified coordinate achored at the first frame.

### 5.2 Comparisons with Other Methods

**ScanNet** To evaluate the results quality, we use the depth error suggested in [15]. The error in camera motion is measured by the rotation error (the minimum rotation to align the ground truth

	Ours	Ours*	DeMoN*	Photometric BA	Geometric BA
Rotation (degree)	<b>1.018</b>	1.587	3.791	4.409	8.56
Translation (cm)	<b>3.39</b>	10.81	15.5	21.40	36.995
Translation (degree)	<b>20.577</b>	31.005	31.626	34.36	39.392
abs relative difference	<b>0.161</b>	0.238	0.231	0.268	0.382
sqr relative difference	<b>0.092</b>	0.176	0.520	0.427	1.163
RMSE (linear)	<b>0.346</b>	0.488	0.761	0.788	0.876
RMSE (log)	<b>0.214</b>	0.279	0.289	0.330	0.366
RMSE (log, scale inv.)	<b>0.184</b>	0.276	0.284	0.323	0.357

Table 1: Quantitative Comparisons with DeMoN and classic BA. The superindex \* denotes that the model is trained on the training set described in [50].

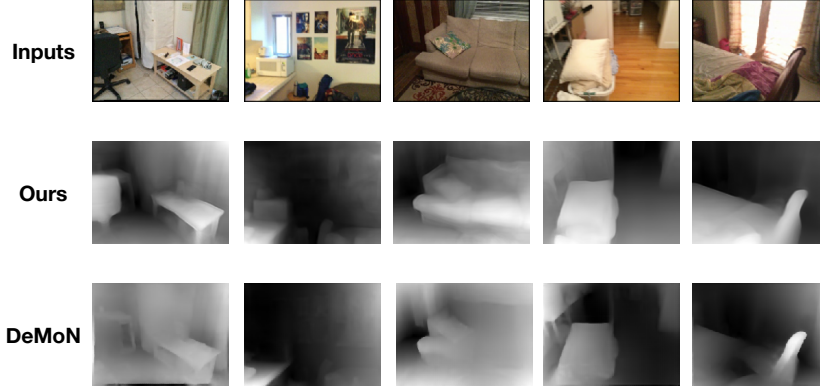


Figure 5: Qualitative Comparisons with DeMoN [50].

and estimated camera coordinate axes), the translation direction error (the angle between ground truth and estimated relative camera translation direction), the absolute position error (the distance between ground truth and estimated camera center point). In Table 1, we compare our method with DeMoN [50]. Note that we cannot get DeMoN trained on our data. For fair comparison, we train our network on the same training data as DeMoN and test both networks on our testing data. We also show the results of our network trained on our own training data. Our BA-Net consistently performs better than DeMoN no matter which training data is used. Since DeMoN does not recover the absolute scale, we align its depth map with the groundtruth to recover its metric scale. We further compare with conventional methods with geometric [37, 2] and photometric [18] BA. Again, our method produces better results. For geometric BA, the reason is that feature matching is difficult because indoor scenes lack rich textures, which makes the geometric error in Equation (1) unreliable. While for photometric BA, it is because the highly non-convex objective function is difficult to optimize as described in Section 3.

**KITTI** For depth evaluation, we use the same metrics as for comparisons on ScanNet. Our method outperforms the supervised methods [16, 34, 22] as well as recent unsupervised methods [56, 8, 22]. As shown in Figure 6, our method recovers more detailed and accurate depth maps than [8] and [22]. Table 2 shows that our method also achieves more accurate camera motion estimation than the methods [56, 8]. We believe this is due to our ‘feature BA’ with features learned specifically for SfM problem, which makes the objective function closer to convex and easier to optimize as discussed in Section 3. In comparison, the methods in [56, 8] minimize the photometric loss.

	Ours	Wang et al [8]	Zhou et al [56]	Godard et al [22]	Liu et al [34]	Eigen et al [16]
ATE(km)	<b>0.019</b>	0.045	0.063	N/A	N/A	N/A
abs rel	<b>0.083</b>	0.151	0.208	0.148	0.202	0.203
sqr rel	<b>0.025</b>	1.257	1.768	1.344	1.614	1.548
RMSE(linear)	<b>3.640</b>	5.583	6.856	5.927	6.523	6.307
RMSE(log)	<b>0.134</b>	0.228	0.283	0.247	0.275	0.282

Table 2: Quantative Comparison on KITTI.



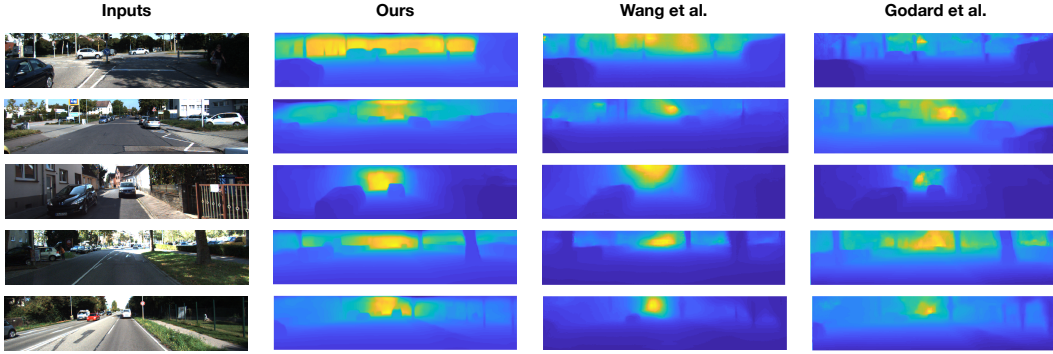


Figure 6: Qualitative Comparisons with Wang et al. [8] and Godard et al [22].

	Ours (Full)	w/o Feature Learning	w/o BA Optimization	w/o $\lambda$ Prediction
Rotation (degree)	<b>1.018</b>	2.667	1.036	3.176
Translation (cm)	<b>3.39</b>	10.8	3.91	12.83
Translation (degree)	<b>20.577</b>	31.493	26.779	31.905
abs relative difference	<b>0.161</b>	0.267	0.217	0.259
sqr relative difference	<b>0.092</b>	0.242	0.145	0.549
RMSE (linear)	<b>0.346</b>	0.481	0.428	0.557
RMSE (log)	<b>0.214</b>	0.303	0.270	0.345
RMSE (log, scale inv.)	<b>0.184</b>	0.226	0.205	0.306

Table 3: Ablation Study Comparisons by Disabling Different Components of BA-Net

### 5.3 Ablation Studies

**Learned Features vs Pre-trained Features** Our learned feature pyramid improves the convexity of the objective function to facilitate the optimization. We compare our learned feature with features pre-trained on ImageNet for classification tasks. As shown in Table 3, the pretrained feature produces larger error. This proves the discussion in Section 4.2.

**Bundle Adjustment Optimization vs SE(3) Pose Estimation** Our BA-Layer optimizes depth and camera poses jointly. We compare it to the SE(3) camera pose estimation with fixed depth map (generated by a monocular image depth estimation method), which is adopted in [8]. To make the comparison fair, we also use our learned feature for the SE(3) camera pose estimation. As shown in Table 3, without BA optimization, both the depth maps and camera poses are worse, because the errors in the depth estimation will degrade the camera pose estimation.

**Differentiable LM vs Damped Gauss Newton(with out  $\lambda$  prediction)** To make the whole pipeline end-to-end trainable, we make the LM algorithm differentiable by learning the damping factor from neural networks. We compare our method with the damped Gauss-Newton which is used in [6]. In damped Gauss Newton algorithm the damping factor  $\lambda$  is prefixed. Again, for fair comparison, we provide our learned feature pyramids to both methods, though it cannot be learned without our differentiable method. As shown in Table 3, our method works much better, because the fixed  $\lambda$  is not optimal for all iterations, and the update could make the solution moves to the wrong direction.

## 6 Conclusions and Future Works

This paper presents the BA-Net, a network that explicitly enforces multi-view geometry constraints in terms of feature reprojection error. It optimizes scene depth and camera motion together via bundle adjustment. The whole pipeline is differentiable and thus end-to-end trainable, such that the features are learned from data to facilitate structure-from-motion. The dense depth is parameterized as a linear combination of some bases depth maps generated from the network. Our BA-Net nicely combines domain knowledge (hard-coded multi-view geometry constraint) with machine learning (learned feature representation and bases depth map generator). It outperforms conventional BA and recent deep learning based methods. Although we only demonstrate it with two-view reconstruction here, it is readily to be generalized to multiple views.

## References

- [1] S. Agarwal, Y. Furukawa, N. Snavely, I. Simon, B. Curless, S. M. Seitz, and R. Szeliski. Building rome in a day. *Commun. ACM*, 54(10):105–112, Oct. 2011.
- [2] S. Agarwal, K. Mierle, and Others. Ceres solver. <http://ceres-solver.org>.
- [3] S. Agarwal, N. Snavely, S. M. Seitz, and R. Szeliski. Bundle adjustment in the large. In *Proceedings of the 11th European Conference on Computer Vision: Part II, ECCV’10*, pages 29–42, Berlin, Heidelberg, 2010. Springer-Verlag.
- [4] B. Amos and J. Z. Kolter. OptNet: Differentiable optimization as a layer in neural networks. In *Proceedings of the 34th International Conference on Machine Learning*, volume 70 of *Proceedings of Machine Learning Research*, pages 136–145. PMLR, 2017.
- [5] C. Beder and R. Steffen. Determining an initial image pair for fixing the scale of a 3d reconstruction from an image sequence. In K. Franke, K.-R. Müller, B. Nickolay, and R. Schäfer, editors, *Pattern Recognition*, pages 657–666, Berlin, Heidelberg, 2006. Springer Berlin Heidelberg.
- [6] M. Bloesch, J. Czarnowski, R. Clark, S. Leutenegger, and A. J. Davison. Codeslam - learning a compact, optimisable representation for dense visual SLAM. *CoRR*, abs/1804.00874, 2018.
- [7] D. Brown. *A Solution to the General Problem of Multiple Station Analytical Stereotriangulation*. RCA Data reduction technical report. D. Brown Associates, Incorporated, 1958.
- [8] M. J. R. Z. S. L. Chaoyang Wang, Buenaposada. Learning depth from monocular videos using direct methods. In *2018 IEEE Conference on Computer Vision and Pattern Recognition (CVPR)*, 2018.
- [9] J. Czarnowski, S. Leutenegger, and A. J. Davison. Semantic texture for robust dense tracking. In *2017 IEEE International Conference on Computer Vision Workshops (ICCVW)*, pages 851–859, Oct 2017.
- [10] A. Dai, A. X. Chang, M. Savva, M. Halber, T. Funkhouser, and M. Nießner. Scannet: Richly-annotated 3d reconstructions of indoor scenes. In *2017 IEEE Conference on Computer Vision and Pattern Recognition (CVPR)*, pages 2432–2443, July 2017.
- [11] A. Delaunoy and M. Pollefeys. Photometric bundle adjustment for dense multi-view 3d modeling. In *2014 IEEE Conference on Computer Vision and Pattern Recognition*, pages 1486–1493, June 2014.
- [12] J. Domke. Generic methods for optimization-based modeling. In *AISTATS*, 2012.
- [13] C. Dong, C. C. Loy, K. He, and X. Tang. Image super-resolution using deep convolutional networks. *IEEE Transactions on Pattern Analysis and Machine Intelligence*, 38(2):295–307, Feb 2016.
- [14] A. Dosovitskiy, P. Fischer, E. Ilg, P. Hausser, C. Hazirbas, V. Golkov, P. van der Smagt, D. Cremers, and T. Brox. FlowNet: Learning optical flow with convolutional networks. In *The IEEE International Conference on Computer Vision (ICCV)*, December 2015.
- [15] D. Eigen and R. Fergus. Predicting depth, surface normals and semantic labels with a common multi-scale convolutional architecture. In *2015 IEEE International Conference on Computer Vision (ICCV)*, pages 2650–2658, Dec 2015.
- [16] D. Eigen, C. Puhrsch, and R. Fergus. Depth map prediction from a single image using a multi-scale deep network. In *Proceedings of the 27th International Conference on Neural Information Processing Systems - Volume 2, NIPS’14*, pages 2366–2374, Cambridge, MA, USA, 2014. MIT Press.
- [17] J. Engel, V. Koltun, and D. Cremers. Direct sparse odometry. *IEEE Transactions on Pattern Analysis and Machine Intelligence*, PP(99):1–1, 2017.
- [18] J. Engel, T. Schöps, and D. Cremers. Lsd-slam: Large-scale direct monocular slam. In *Proc. of ECCV*, 2014.

- [19] J. Engel, V. C. Usenko, and D. Cremers. A photometrically calibrated benchmark for monocular visual odometry. *CoRR*, abs/1607.02555, 2016.
- [20] A. Geiger, P. Lenz, and R. Urtasun. Are we ready for autonomous driving? the kitti vision benchmark suite. In *Conference on Computer Vision and Pattern Recognition (CVPR)*, 2012.
- [21] A. Geiger, J. Ziegler, and C. Stiller. Stereoscan: Dense 3d reconstruction in real-time. In *Intelligent Vehicles Symposium (IV)*, 2011.
- [22] C. Godard, O. Mac Aodha, and G. J. Brostow. Unsupervised monocular depth estimation with left-right consistency. In *CVPR*, 2017.
- [23] A. Handa, M. Bloesch, V. Pătrăucean, S. Stent, J. McCormac, and A. Davison. *gvnn: Neural Network Library for Geometric Computer Vision*, pages 67–82. Springer International Publishing, Cham, 2016.
- [24] K. He, X. Zhang, S. Ren, and J. Sun. Deep residual learning for image recognition. In *2016 IEEE Conference on Computer Vision and Pattern Recognition (CVPR)*, pages 770–778, June 2016.
- [25] D. Hoiem, A. A. Efros, and M. Hebert. Automatic photo pop-up. In *ACM SIGGRAPH 2005 Papers*, SIGGRAPH ’05, pages 577–584, New York, NY, USA, 2005. ACM.
- [26] G. Huang, Z. Liu, L. van der Maaten, and K. Q. Weinberger. Densely connected convolutional networks. In *The IEEE Conference on Computer Vision and Pattern Recognition (CVPR)*, July 2017.
- [27] E. Ilg, N. Mayer, T. Saikia, M. Keuper, A. Dosovitskiy, and T. Brox. FlowNet 2.0: Evolution of optical flow estimation with deep networks. In *The IEEE Conference on Computer Vision and Pattern Recognition (CVPR)*, July 2017.
- [28] A. Kendall, H. Martirosyan, S. Dasgupta, P. Henry, R. Kennedy, A. Bachrach, and A. Bry. End-to-end learning of geometry and context for deep stereo regression. *CoRR*, abs/1703.04309, 2017.
- [29] D. P. Kingma and J. Ba. Adam: A method for stochastic optimization. *CoRR*, abs/1412.6980, 2014.
- [30] A. Krizhevsky, I. Sutskever, and G. E. Hinton. Imagenet classification with deep convolutional neural networks. In F. Pereira, C. J. C. Burges, L. Bottou, and K. Q. Weinberger, editors, *Advances in Neural Information Processing Systems 25*, pages 1097–1105. Curran Associates, Inc., 2012.
- [31] L. Ladický, J. Shi, and M. Pollefeys. Pulling things out of perspective. In *Proceedings of the 2014 IEEE Conference on Computer Vision and Pattern Recognition*, CVPR ’14, pages 89–96, Washington, DC, USA, 2014. IEEE Computer Society.
- [32] I. Laina, C. Rupprecht, V. Belagiannis, F. Tombari, and N. Navab. Deeper depth prediction with fully convolutional residual networks. In *2016 Fourth International Conference on 3D Vision (3DV)*, pages 239–248, Oct 2016.
- [33] T. Y. Lin, P. Dollár, R. Girshick, K. He, B. Hariharan, and S. Belongie. Feature pyramid networks for object detection. In *2017 IEEE Conference on Computer Vision and Pattern Recognition (CVPR)*, pages 936–944, July 2017.
- [34] F. Liu, C. Shen, G. Lin, and I. Reid. Learning depth from single monocular images using deep convolutional neural fields. *IEEE Transactions on Pattern Analysis and Machine Intelligence*, 38(10):2024–2039, Oct 2016.
- [35] M. L. A. Lourakis and A. A. Argyros. Is levenberg-marquardt the most efficient optimization algorithm for implementing bundle adjustment? In *Tenth IEEE International Conference on Computer Vision (ICCV’05) Volume 1*, volume 2, pages 1526–1531 Vol. 2, Oct 2005.
- [36] R. Mur-Artal, J. M. M. Montiel, and J. D. Tardós. Orb-slam: a versatile and accurate monocular slam system. *IEEE Trans. Rob.*, 31:1147–1163, 2015.

- [37] D. Nister. An efficient solution to the five-point relative pose problem. *IEEE Transactions on Pattern Analysis and Machine Intelligence*, 26(6):756–770, June 2004.
- [38] J. Nocedal and S. J. Wright. *Numerical Optimization*. Springer, New York, 2nd edition, 2006.
- [39] J. Pang, W. Sun, J. Ren, C. Yang, and Q. Yan. Cascade Residual Learning: A Two-stage Convolutional Neural Network for Stereo Matching. *ArXiv e-prints*, Aug. 2017.
- [40] A. Saxena, S. H. Chung, and A. Y. Ng. Learning depth from single monocular images. In *Proceedings of the 18th International Conference on Neural Information Processing Systems*, NIPS’05, pages 1161–1168, Cambridge, MA, USA, 2005. MIT Press.
- [41] A. Saxena, M. Sun, and A. Y. Ng. Make3d: Learning 3d scene structure from a single still image. *IEEE Transactions on Pattern Analysis and Machine Intelligence*, 31(5):824–840, May 2009.
- [42] U. Schmidt and S. Roth. Shrinkage fields for effective image restoration. In *2014 IEEE Conference on Computer Vision and Pattern Recognition*, pages 2774–2781, June 2014.
- [43] J. L. Schönberger and J.-M. Frahm. Structure-from-motion revisited. In *IEEE Conference on Computer Vision and Pattern Recognition (CVPR)*, 2016.
- [44] K. Simonyan and A. Zisserman. Very deep convolutional networks for large-scale image recognition. *CoRR*, abs/1409.1556, 2014.
- [45] F. Steinbruecker, J. Sturm, and D. Cremers. Real-time visual odometry from dense rgb-d images. In *Workshop on Live Dense Reconstruction with Moving Cameras at the Intl. Conf. on Computer Vision (ICCV)*, 2011.
- [46] C. Tang, O. Wang, and P. Tan. Gslam: Initialization-robust monocular visual slam via global structure-from-motion. In *2017 Fifth International Conference on 3D Vision (3DV)*, pages 239–248, Oct 2017.
- [47] K. Tateno, F. Tombari, I. Laina, and N. Navab. Cnn-slam: Real-time dense monocular slam with learned depth prediction. In *2017 IEEE Conference on Computer Vision and Pattern Recognition (CVPR)*, pages 6565–6574, July 2017.
- [48] B. Triggs, P. F. McLauchlan, R. I. Hartley, and A. W. Fitzgibbon. Bundle adjustment - a modern synthesis. In *Proceedings of the International Workshop on Vision Algorithms: Theory and Practice*, ICCV ’99, pages 298–372, London, UK, UK, 2000. Springer-Verlag.
- [49] B. Triggs, P. F. McLauchlan, R. I. Hartley, and A. W. Fitzgibbon. Bundle adjustment - a modern synthesis. In *Proceedings of the International Workshop on Vision Algorithms: Theory and Practice*, ICCV ’99, pages 298–372, London, UK, UK, 2000. Springer-Verlag.
- [50] B. Ummenhofer, H. Zhou, J. Uhrig, N. Mayer, E. Ilg, A. Dosovitskiy, and T. Brox. Demon: Depth and motion network for learning monocular stereo. In *The IEEE Conference on Computer Vision and Pattern Recognition (CVPR)*, July 2017.
- [51] C. Wu, S. Agarwal, B. Curless, and S. M. Seitz. Multicore bundle adjustment. In *CVPR 2011*, pages 3057–3064, June 2011.
- [52] S. "Xie and Z. Tu. Holistically-nested edge detection. In *Proceedings of IEEE International Conference on Computer Vision*, 2015.
- [53] D. Xu, E. Ricci, W. Ouyang, X. Wang, and N. Sebe. Multi-scale continuous crfs as sequential deep networks for monocular depth estimation. In *2017 IEEE Conference on Computer Vision and Pattern Recognition (CVPR)*, pages 161–169, July 2017.
- [54] D. Xu, E. Ricci, W. Ouyang, X. Wang, and N. Sebe. Multi-scale continuous crfs as sequential deep networks for monocular depth estimation. In *2017 IEEE Conference on Computer Vision and Pattern Recognition (CVPR)*, pages 161–169, July 2017.
- [55] F. Yu, V. Koltun, and T. Funkhouser. Dilated residual networks. In *2017 IEEE Conference on Computer Vision and Pattern Recognition (CVPR)*, pages 636–644, July 2017.

- [56] T. Zhou, M. Brown, N. Snavely, and D. G. Lowe. Unsupervised learning of depth and ego-motion from video. In *The IEEE Conference on Computer Vision and Pattern Recognition (CVPR)*, July 2017.
- [57] L. Zwald and S. Lambert-Lacroix. The BerHu penalty and the grouped effect. *ArXiv e-prints*, jul 2012.